Soil Dynamics and Earthquake Engineering 161 (2022) 107393

Contents lists available at ScienceDirect

Soil Dynamics and Earthquake Engineering

journal homepage: www.elsevier.com/locate/soildyn

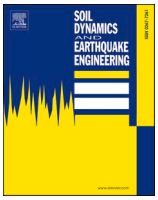

Numerical model for dynamic installation of large diameter monopiles

Amir M. Kaynia [a,c,*], Jan Hebig [b], Taisiya Pein [b], Yunsup Shin [d]

[a] Norwegian University of Science and Technology (NTNU), Trondheim, Norway
[b] Fraunhofer-Institute for Wind Energy Systems IWES, Bremen, Germany
[c] Norconsult AS, Sandvika, Norway
[d] Norwegian Geotechnical Institute, Oslo, Norway

A B S T R A C T

This paper presents the numerical code *VibPile* for simulation of the nonlinear dynamic response of large monopiles under harmonic loading and installation by vibration or impact driving. *VibPile* is based on a nonlinear FE model of the pile-soil interaction along the shaft and the tip by elasto-plastic springs representing the near field and elasto-dynamic elements (spring and dashpot) for the far field. While for the shaft friction and tip resistance the classical engineering solutions, such as those by standards or guidelines (e.g. API) and literature, are used in the numerical simulations, new computational models are developed for the dynamic response of the soil inside the pile and the far-field elasto-dynamic springs.

What primarily differentiates the present model from the existing ones is the treatment of the soil inside the monopile together with the stiffness at the pile tip. Most existing models are based on the solutions for piles with solid sections or pipe piles in which the soil inside the pile follows the pile vibrations like a solid section. For large diameter monopiles commonly used for offshore wind turbines, both the soil response inside the pile and the stiffness of the pile tip are different. The developed model is verified against the vibro-pile test data collected at Altenwalde, Germany. The results include axial pile strains, accelerations, and shear stresses along the pile shaft and at the pile tip. Both the strains and accelerations as well as the rate of pile driving measured at Altenwalde are reproduced by *VibPile* with reasonable accuracy. Sensitivity analyses are presented to highlight the effects of the shear wave velocity and shear strength at the pile-soil interface on the pile driving rate. Moreover, the effect of the natural period of the inner soil on the pile driving is investigated.

1. Introduction

Dynamic pile testing is carried out during impact pile driving to gain an estimate of the static pile capacity. The procedure in general consists of recording the axial pile strain and accelerations near the pile head during hammer strikes and using them to determine the simultaneous time histories of the force and particle velocity in the pile. Pile capacity is then computed from a numerical model of the pile based on 1D wave propagation in the pile-soil system [e.g. 1]. A best matching between the force and the particle velocity, V, times the pile's impedance, Z, in an iterative process, often referred to as signal matching, is then used to estimate the soil parameters. Most of the existing tools, such as CAPWAP [2] and IMPACT [3] are based on either the Smith's finite difference method [1] or the method of characteristics [4]. Other tools such as GRLWEAP [5] that have been developed on the same principles are used for construction control for a particular required capacity that give, for a range of hammer strokes or energy levels, minimum required blow count and the associated stress levels.

The methods based on 1D FE dynamic models of the pile often discretize the pile into lumped masses with discrete linear springs representing the axial pile stiffness. The pile-soil interaction is often represented by a series of elasto-plastic springs, representing the nonlinear soil response at the pile interface, together with elastic springs and dashpots for capturing the dynamics of the far field including radiation damping. A conceptually similar model is used in the present study for pile-soil interaction as shown schematically in Fig. 1. The parameters of the springs and dashpots along the pile are dependent on the soil properties which vary with depth and soil stratification.

For the far-field response, most of the existing methods use the analytical expressions for the dynamic response of 2D solids in polar coordinates derived by Baranov [6] and later adapted by Novak [7] for dynamic analysis of piles. This model considers only the wave propagation outside the pile and is strictly speaking valid for solid piles; moreover, the waves are assumed to propagate only horizontally at each point and independently of each other, hence a dynamic Winkler model. Numerous attempts have been made over the years to simplify these expressions or extend them to non-homogeneous soil profiles [8,9]. The reader is referred to Ref. [10] for a comprehensive review of the literature with focus on analytical and simplified solutions in the frequency domain. The advantage of frequency domain solutions is the possibility of rigorously accounting for the radiation damping. Realizing the importance of this property on the dynamic response, attempts have been made to adapt the analytical solutions to those in which the soil

* Corresponding author. Norwegian University of Science and Technology (NTNU), Trondheim, Norway.
E-mail address: amir.kaynia@ntnu.no (A.M. Kaynia).

https://doi.org/10.1016/j.soildyn.2022.107393
Received 25 January 2022; Received in revised form 6 June 2022; Accepted 10 June 2022
Available online 9 July 2022

Symbols and abbreviations

a	Pile radius
a_0	Non-dimensional frequency, $\omega d/V_s$
API	American Petroleum Institute
C	Damping matrix of pile-soil system
C_b	Radiation damping at pile tip
C_S	Radiation damping at pile shaft
d	Pile diameter $= 2a$
f	Unit skin friction at pile shaft
f_b	Yield force of soil at pile tip
f_{su}	Yield force at shaft-soil interface due to skin friction
G	Shear modulus of soil
$H_0^{(2)}$	Hankel function of second kind
J_0 and J_1	Bessel functions of first kind
k	Wavenumber
K_l	Lateral earth pressure on shaft
K_b^{ep}	Elasto-plastic pile tip-soil spring
K_b^e	Elastic stiffness of pile tip-soil spring
K_s^{ep}	Elasto-plastic shaft-soil spring
K_s^e	Elastic stiffness of shaft-soil spring
K	Stiffness matrix of pile-soil system
M	Mass matrix of pile-soil system
N_q	Bearing capacity factor
q_{tip}	CPT tip resistance
r	Radial distance from centre of pile
SDMT	Seismic dilatometer
t	Wall thickness of pile
U	Vector of vertical pile displacements
V	Axial particle velocity in pile
V_s	Shear wave velocity of soil
w	Vertical displacement of soil inside pile
Z	Pile section impedance
α	Shaft-soil stiffness normalized by G
β	Shaft-soil damping normalized by Gd/V_s
δ	Pile-soil friction angle
ζ	Pile tip-soil damping normalized by Gd/V_s
η	Pile tip-soil stiffness normalized by Gd
ρ	Mass density of soil
σ'_{v0}	Effective vertical stress in soil
φ	Internal friction angle of soil
ω	Vibration frequency (rad/s)

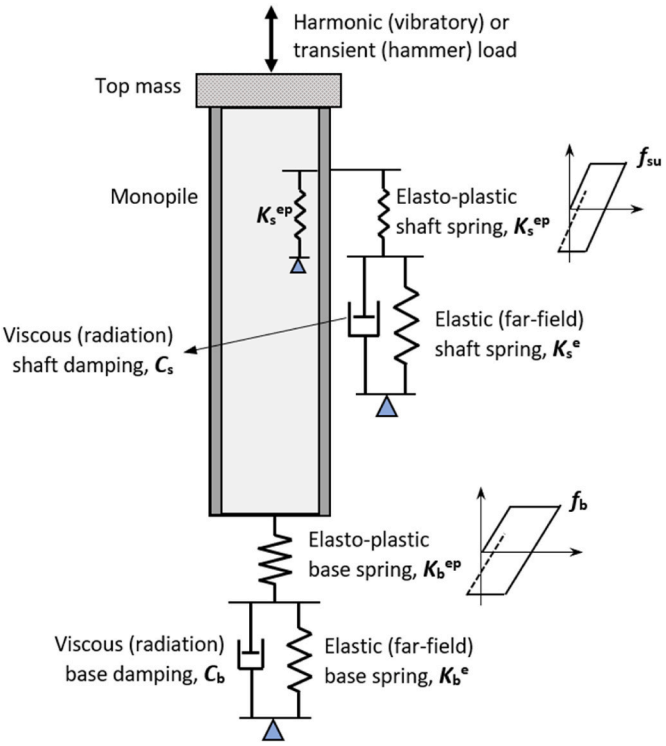

Fig. 1. Schematics of simple mechanical soil-monopile interaction during dynamic installation.

nonlinearity at or adjacent the pile interface is incorporated in an equivalent linear manner [11]. While such methods have improved the understanding of the dynamic response of piles in nonlinear soil, they are not able to provide a good estimate of pile penetration during vibration.

Therefore, the main focus on dynamic pile-soil interaction in pile driving has been on development of discrete models that can handle the nonlinear near field response while taking advantage of the wealth of models for the far field. These models have invariably been formulated in the time domain in which the far field is represented by an elastic spring and a viscous dashpot representing radiation damping. Various adaptations have been introduced in these models, for example inclusion of added soil mass [12,13] or representation of the near field by hysteretic models which update the nonlinear pile-soil behaviour using data for soil modulus reduction and damping as function of shear strain. See Ref. [14] for a comprehensive review of the methods based on this approach. The pile tip has also received a fair attention due to the complexity of the pile-soil interaction at this point during loading and unloading phases and possibility of separation. A sophisticated model has been advanced for this mechanism [15], however, it is not clear how important this mechanism is on the overall pile driving response, especially at larger depths.

The literature on the subject is very rich and covers many aspects, including both analytical and practical issues. The reader is referred to several state-of-the-art publications [e.g. 16], which in addition to the above modelling issues, address the wave propagation from pile driving and their impact on the surrounding built environment.

The objective of the present study is to develop a numerical simulation model, *VibPile*, based on the principles presented in Fig. 1. While this model has many similarities with other models, as presented above, this study focuses on the effect of vibration of the soil inside the pile on the pile-soil dynamic mechanism. To the knowledge of the authors, all existing solutions are based on the dynamic solution in Ref. [7] or its variations which assume a solid pile section. In monopiles with diameters as large as 10 m (which keep on increasing), the wavelengths of the soil inside the monopile at large vibration frequencies could be of the same order as the diameter of the pile. This could excite the axisymmetric vibration modes which in turn affect the dynamics of the pile. The loading condition is also different at the pile tip as the load acts on a thin ring compared to disk loads in the case of solid piles. Both these issues are studied in the following and typical parameters are derived for practical design. The results of the present model are benchmarked against the large-scale vibro-piling tests performed in Altenwalde, Germany.

2. Test site and data

The pile driving tests (Fig. 2) were carried out as part of the joint industry and research project *Vibro-Project* [17] coordinated by the

Fig. 2. Pile driving by vibration at Altenwalde [17].

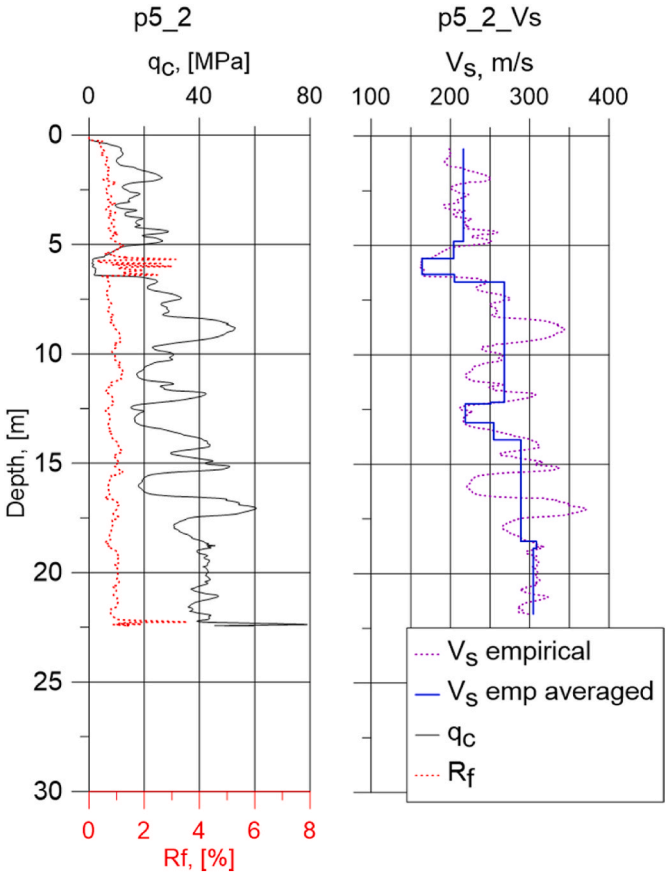

Fig. 3. Estimated shear wave velocity profiles at CPT location (p5_2) close to pile P5.

Vibro Pile Consortium in 2014. The project has been a major research endeavour with the main goal of studying monopile installation, and comprised, among others, site characterization at the test site, large-scale pile driving by vibration, effect of vibration on soil properties, attenuation of vibration in soil with distance, data collection/analysis, and numerical simulation of pile driving using advanced FE tools. Development of a simple numerical simulation tool, as carried out in the present study, was considered complementary to the advanced analyses.

The ground in the area is characterized by sandy, mostly very dense soils, and the groundwater level is approximately at 4 m depth. Prior to the pile installation, a thorough site investigation campaign was carried out which comprised 30 CPTs and two sampling boreholes. The subsoil is comparable to the soil conditions at many North Sea Projects in the German Bight.

Three pairs of monopiles with diameter $d = 4.3$ m and length $L = 21$ m were installed by impact and vibrational driving techniques. Table 1 lists the vibratory driving parameters for the three tested piles (identified as P1v, P4v and P5v). In this study we consider the vibratory driven pile P5 with the driven depth of 18.80 m.

The shear wave velocity, *Vs*, was estimated using CPT correlations and is idealized by a piecewise constant profile as shown in Fig. 3.

Shear wave velocities were also measured in a follow-up research project at two nearby locations using seismic dilatometer SDMT and cross-hole tests which generally confirmed the interpretation shown in Fig. 3. More details about the shear velocity measurements can be found in Ref. [18].

3. Numerical model

Fig. 4 presents the schematics of the problem under consideration. The load is applied by rotation of eccentric masses in a top-mounted vibro-hammer. This load is resisted by the shaft friction and pile-tip reaction. Due to the large diameter of typical monopiles used offshore, it is expected that the piles are installed in unplugged condition. Therefore, the tip resistance is derived from the soil reaction against the annulus of pile wall as shown in the figure.

The following sections describe the various elements of this model. The stiffness and dashpot/damping constants are derived analytically based on dynamics of the far-field response, and the soil strength values (at pile shaft and tip) are based on conventional pile driving formula available in various standards and literature. It is not in the scope of this study to develop models for determining these parameters nor evaluating the accuracy of the employed models. However, the adopted formula/solutions for sand from API are included for completeness.

Table 1
Vibratory driving parameters.

Pile	units	P1v		P4v		P5v	
Depth	m	<9.5 m	>9.5 m	<8.5 m	>8.5 m	<9.5 m	>9.5 m
Frequency	Hz	12	22.5/15	12	22.5	12	22.5
Vibration power	bar	150–200	380	200–300	380	200–300	380

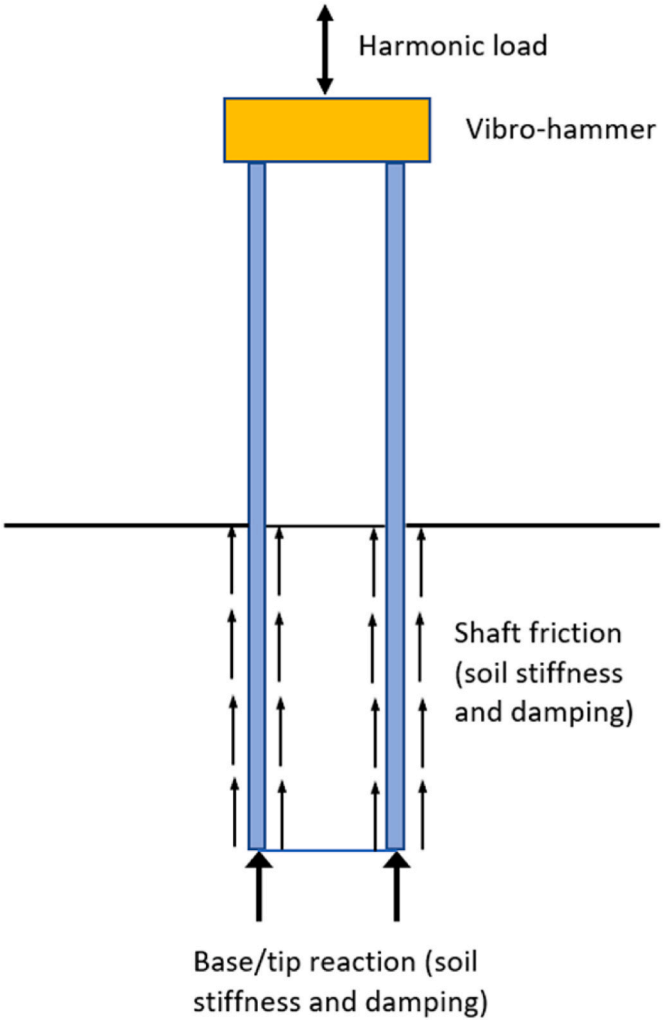

Fig. 4. Key features of monopile/soil model and vibro-hammer.

3.1. Stiffness and damping

This section derives new formulas for stiffness and damping of pile-soil springs along the pile shaft and at the pile tip using analytical models. To the authors' knowledge, all existing solutions are based on models developed for solid piles; therefore, they are not theoretically applicable for large-diameter hollow/pipe piles. The analyses presented in this section clearly show the significant effect of the waves in the soil inside the pile on the characteristics of monopile response.

3.1.1. Pile-shaft dynamic stiffness

Fig. 5 shows pile-soil interaction forces in a uniform soil medium due to vertical vibration. The forces represent the sum of those inside and outside of the pile shaft. To compute the pile response to these loads the rigorous elasto-dynamic model PILES [19] was used. A uniform soil medium together with a long rigid monopile was considered for the computations. This simulates a condition close to the case used in Winkler models [7] which are often used to derive the stiffness and damping per unit pile length as function of the soil's shear modulus and pile diameter. To represent practical cases, two pile diameters were considered: i) $d = 4.3$ m (used in the pile tests), and ii) $d = 10$ m representing currently designed large monopiles for offshore wind turbines.

The analyses in PILES are carried out in the frequency domain. From the applied stresses and computed displacements at the pile wall, one can derive pile-soil dynamic stiffnesses which are complex quantities. The real part of the dynamic stiffness represents the combined effect of

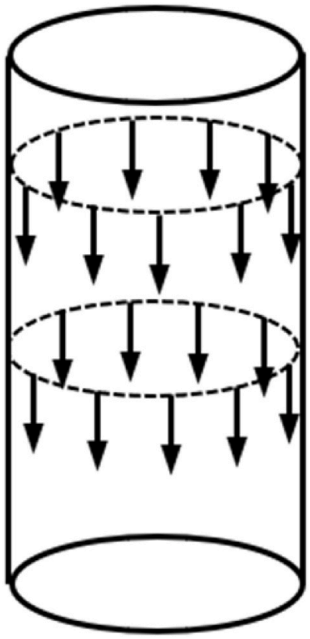

Fig. 5. Ring soil tractions in infinite soil medium representing pile-soil interaction.

static stiffness and added soil mass (inside and outside of the pile) and the imaginary part, when divided by frequency, represents the radiation damping. While the analyses were performed for a typical average shear wave velocity $Vs = 250$ m/s and mass density $\rho = 2000$ kg/m^3 (hence, shear modulus, $G = 125$ MPa), one can use them for other Vs values by normalizing the results by G, as described in the following.

Fig. 6 presents the variation with circular frequency, ω, of the normalized computed stiffness per unit pile length, α, and the corresponding normalized damping, β, for the two pile diameters 4.3 m and 10 m. The normalization of the stiffness is with G (hence, the absolute value of stiffness per unit pile length is $\alpha \cdot G$). The normalization of the damping is with $G \cdot d/Vs$, that is, the equivalent dashpot constant per unit length (C_s in Fig. 1) is $\beta \cdot G \cdot d/Vs$.

There are a few interesting points to note in this figure.

1. The results for the two pile diameters look generally similar if the frequency is normalized by the pile diameter, d, and shear wave velocity so that the axis reflects the number of wavelengths inside the monopile. This is confirmed by the plots in Fig. 7 which shows the same results as function of the conventional nondimensional frequency $a_0 = \omega\, d/Vs$. The peak in the stiffness term indeed corresponds to the first axisymmetric eigenmode of the soil inside the pile in vertical vibration. This is further discussed in the next section. This figure indicates that the results in this nondimensional form could be used for other diameters.
2. The stiffness is strongly dependent on frequency. The values of α at lower frequencies are in the range 3–4 which agree well with the values derived from analytical models [e.g. 7]. However, the figure shows that the stiffness can be considerably larger for frequencies above the eigenfrequency of the inner soil. The results show an increase of about 4-fold. A sharp peak is also observed in the damping term around the eigenfrequency which is discussed in the next section.

3.1.2. Pile-tip dynamic stiffness

Fig. 8 shows the model considered for the computation of the pile-tip dynamic stiffness (that is, stiffness and damping). The analytical model in Ref. [20] was used in the analyses. For this purpose, the contact surface is divided into small elements in the spirit of boundary element

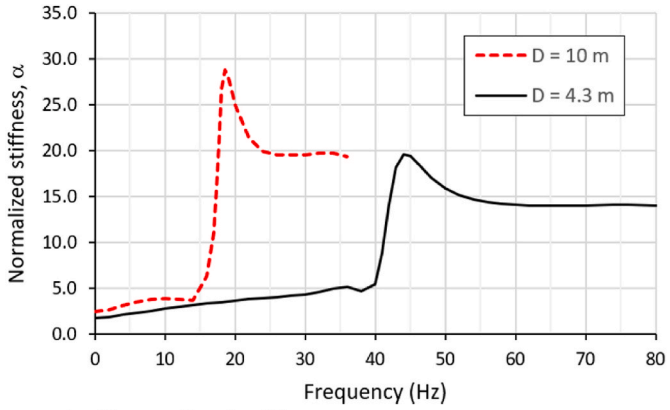

Fig. 6. Normalized vertical stiffness and damping of pile-soil spring as function of frequency.

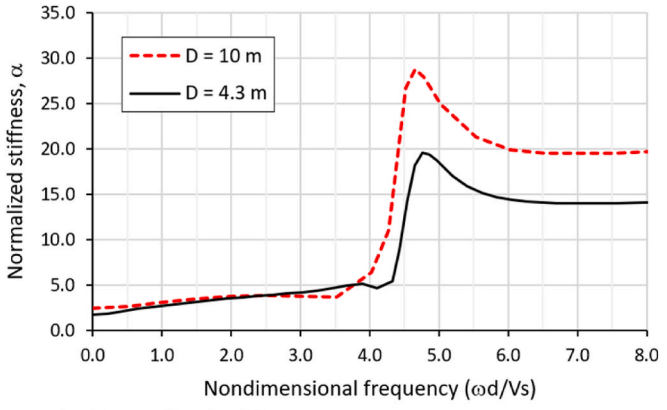

Fig. 7. Normalized vertical stiffness and damping of pile-soil spring per unit pile length as function of non-dimensional frequency a_0.

methods, and the response of the elements in the soil are computed to unit loads applied to the elements. The pile-tip dynamic stiffness is derived by application of the uniform displacements in all the elements. The analyses were again performed for two diameters, namely $d = 4.3$ m, and $d = 10$ m. In both cases the pile wall thickness was taken equal to $d/100$.

Fig. 9 presents the variations of the normalized computed stiffness (η) as function of the nondimensional frequency, a_0, for the case when the load is applied at $z = 10$ m depth. Beyond this depth, the results do not vary noteworthy, therefore, these results could be used for other depths. The normalization of stiffness is with $G{\cdot}d$ (hence, the stiffness is $\eta{\cdot}G{\cdot}d$). As in the case for pile shaft dynamic stiffness, the results for the two pile diameters largely coincide when plotted as function of a_0. The eigenfrequency described above also manifests itself in these results albeit with a less amplification as expected.

Fig. 10 displays the corresponding results for the radiation damping as function of the nondimensional frequency, a_0. The damping values are normalized by $G{\cdot}d^2/Vs$ and presented by ζ, hence, the dashpot constant (C_b in Fig. 1) is $\zeta{\cdot}G{\cdot}d^2/Vs$. The same observation about the similarity of the results when plotted against the non-dimensional frequency applies here as well. For other monopile diameters, one can use a smooth average of the two curves in these figures.

3.1.3. Analytical solution for internal pile shaft stiffness

The analyses in the preceding section revealed presences of a peak at about the natural frequency of the soil inside the monopile and corresponding increase in the pile stiffness and damping. This issue is studied analytically in this section.

The differential equation of motion of the soil for steady-state harmonic vibrations in polar coordinates is given by:

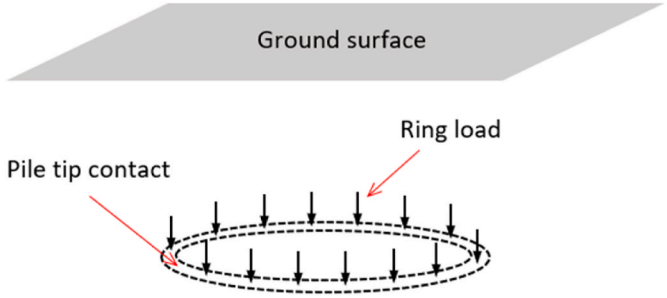

Fig. 8. Representation of loads at pile tip-soil contact at a point below ground surface.

$$\frac{G}{r}\frac{\partial}{\partial r}\left(r\frac{\partial w}{\partial r}\right)+\frac{G}{r^2}\frac{\partial^2 w}{\partial \theta^2}+\rho\omega^2 w=0 \tag{3.1}$$

Where r and θ are the polar coordinates, w is vertical displacement, and ω is frequency of vibration.

For axisymmetric motions, which is the case for vibrations in vertical direction, the second term in Eq. (3.1) is eliminated, and the differential equation is simplified to:

$$\frac{G}{r}\frac{\partial}{\partial r}\left(r\frac{\partial w}{\partial r}\right)+\rho\omega^2 w=0 \tag{3.2}$$

The solution of this equation is Hankel function of the second kind,

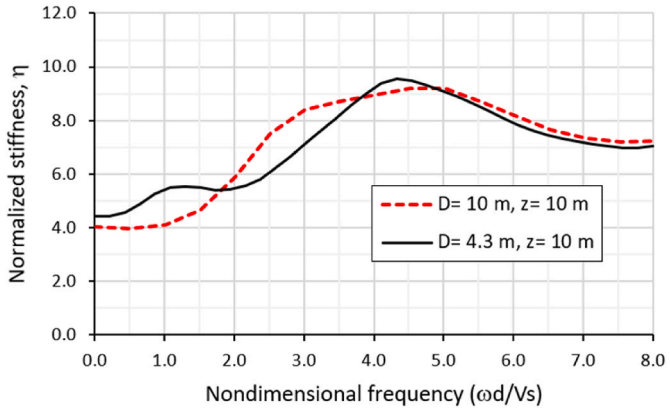

Fig. 9. Normalized vertical stiffness of pile-tip spring as function of frequency.

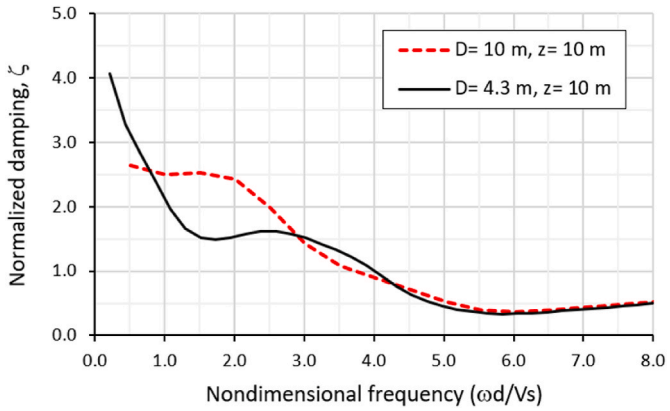

Fig. 10. Normalized damping of pile-tip dashpot as function of frequency.

that is,

$$w(r) = cH_0^{(2)}(kr) \tag{3.3}$$

where $k = \omega/Vs$ is the wave number and c is the solution constant to be determined from the boundary conditions. Considering that the imaginary part in the Hankel function approaches infinity at $r = 0$, the imaginary term should be set to zero, and the solution is further simplified to

$$w(r) = cJ_0(kr) \tag{3.4}$$

Where J_0 is the Bessel function of the 1st kind and order zero. Application of the boundary condition w (at $r = a$) $= w_0$, with w_0 being the pile displacement, leads to the analytical expression for the vibration of the soil inside the pile (note that during the elastic response, there is no slippage at pile-soil interface).

$$w(r) = \frac{w_0}{J_0(ka)} J_0(kr) \tag{3.5}$$

The shear stress in the soil is computed as

$$\tau(r) = G\frac{\partial w}{\partial r} = Gk\frac{w_0}{J_0(ka)} J_1(kr) \tag{3.6}$$

Where J_1 is the Bessel function of the 1st kind and first order. The stiffness of the shaft (for unit pile length) corresponding to the soil response inside the pile can then be computed from the shear force on the shaft and its displacement; that is,

$$K_{\text{internal shaft}} = \pi d\frac{\tau(a)}{w_0} = \pi dk\frac{J_1(ka)}{J_0(ka)} G = \pi a_0 \frac{J_1\left(\frac{a_0}{2}\right)}{J_0\left(\frac{a_0}{2}\right)} G \tag{3.7}$$

The term in front of the shear modulus, G, in this expression can be compared to the normalized stiffness (α) for the external soil in contact with the pile shaft [e.g. 7]. Fig. 11 plots the variations of the two Bessel functions appearing in the above expression.

A very interesting point is that due to the form of the Bessel functions (Fig. 11), the stiffness could theoretically approach infinity at the zeros of J_0. The frequencies corresponding to these zeros are the eigenfrequencies of the axisymmetric eigenmodes of the internal soil as displayed in Fig. 12. It should be noted that the true response will be limited due to soil damping. Soil damping can readily be included in Eq. (3.7) by replacing the shear modulus by its complex counterpart $G^* = G(1 + 2i\xi)$ where ξ is hysteretic damping ratio in the soil.

Fig. 13 displays the stiffness of the internal soil as function of the non-dimensional frequency, a_0, with the same normalization used for the external soil stiffness as plotted in Fig. 7. To be able to plot in logarithmic scale (due to the large values close to the eigenfrequency), the absolute value is plotted. The figure clearly demonstrates the effect of the vibration mode of the soil on the internal soil stiffness. Notice the peak at around $a_0 = 4.7$ and the corresponding peak in Fig. 7a from the PILES computations. In piles with soil inside, this stiffness can be added to the external soil stiffness in traditional Winkler models used in elastodynamic pile solutions [e.g. 7].

3.2. Soil strength parameters

As pointed out earlier, this study does not aim to propose any new method for computation of the soil strength at the pile shaft or pile tip for cyclic loading. Basically, one could use the available methods for computation of these parameters from the existing standards (such as API [21]) or results of various research. Therefore, these methods are not repeated here. However, for completeness and reference, only the method suggested by API for sand (and used in the verification in the next chapter) is included.

3.2.1. Pile shaft and pile tip resistance

According to API, the unit skin friction (pile shaft resistance) can be computed from the following expression:

$$f = K_l\sigma'_{v0}\tan(\delta) \tag{3.8}$$

where.

f = Unit skin friction between pile and soil
K_l = Lateral earth pressure = 0.5 to 1.0 for compressive loading
σ'_{v0} = Effective vertical stress
δ = Soil-pile friction angle (depends on pile surface conditions and generated pore-pressure).

The pile tip resistance can be estimated from

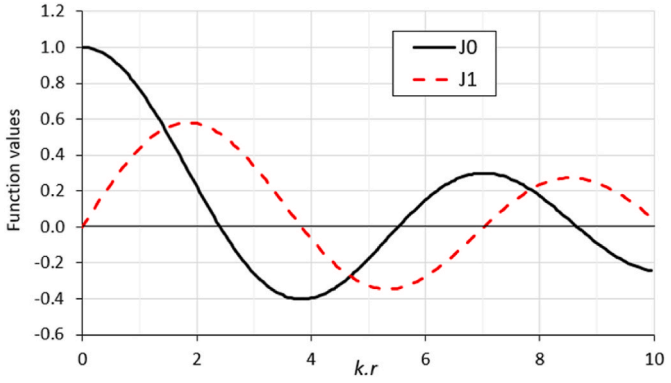

Fig. 11. Variation of Bessel functions J_0 and J_1 as function of kr.

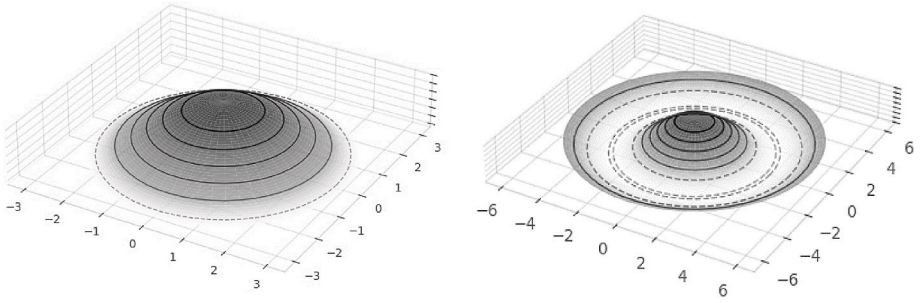

Fig. 12. First and second vibration mode shapes of soil inside monopile; Left: first mode, Right: second mode.

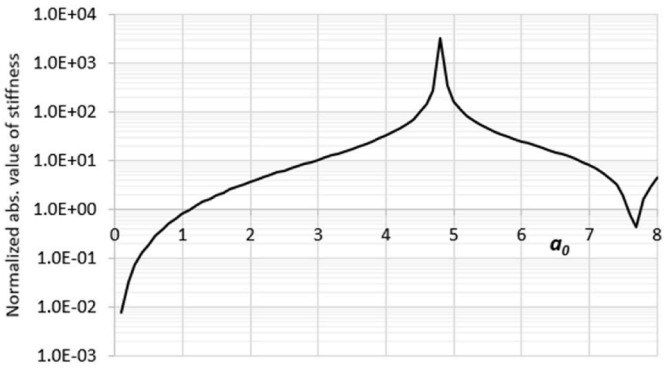

Fig. 13. Variation of normalized internal soil stiffness as function of nondimensional frequency.

$$q_{tip} = \sigma'_{v0} N_q \tag{3.9}$$

where σ'_{v0} is the effective vertical stress and N_q is a bearing capacity factor that depends on the angle of internal friction at the pile-soil interface, φ', and can be computed from the following expressions:

$$for\ \varphi' < 30^\circ : N_q = 11.6\tan^2\left(45^\circ + \frac{\varphi'}{2}\right)\tan(\varphi') \tag{3.10}$$

$$for\ 30^\circ < \varphi' < 35^\circ :\ N_q = 4\,\varphi' - 100 \tag{3.11}$$

$$for\ \varphi' > 35^\circ :\ N_q = 2\,\varphi' - 30\ and\ N_q < 40 \tag{3.12}$$

The tip resistance q_{tip} is limited to:

$$q_{tip,max} = 0.265\,\tan\left(45^\circ + \frac{\varphi'}{2}\right)^{5.5} < 10\ \text{MPa} \tag{3.13}$$

3.3. Solution algorithm

The pile is modelled in *VibPile* by FE beam-column elements with only axial degrees of freedom at the N nodes (hence N-1 pile elements). The load can be a transient force representing a hammer impact or a harmonic (sinusoidal) force representing a vibro-driver acting on the top mass. The differential equation of motion of the model is given by

$$M\ddot{U} + C\dot{U} + KU = F(t) \tag{3.14}$$

Where.

M Mass matrix (dimensions $N \times N$)
K Pile-soil tangent stiffness matrix (dimensions $N \times N$), as function of displacement
C Pile-soil damping matrix (dimensions $N \times N$).
U Vector of incremental nodal displacements (dimensions N)
F Time varying forcing function (dimensions 1)

The incremental form of the above equations was solved by the constant acceleration method which is an implicit and unconditionally stable integration algorithm (e.g. Ref. [22]). The springs representing the pile-soil interaction are assumed elastic-perfectly plastic (Fig. 1). During the part of the response where the soil is yielding, the radiation damping is deactivated.

As stated above, the forcing function can be a transient hammer impact load, or a harmonic load as used during installation by vibration. Because the test data were available for the latter case, the results are presented for a vibratory driving case in the next section.

4. Verification

IWES performed a series of vibro-pile tests at a well characterized site in Altenwalde. The data for the site includes (as interpreted by IWES) friction angle, mass density of soil, shear wave velocity together with the monopile parameters ($d = 4.3$ m, $t = 0.045$ m).

The numerical simulation was carried out for the time the pile had penetrated 10 m in the soil (Fig. 4) because of the good quality of the data around this time. For the stiffness/damping and yield strengths of the 10 soil layers in contact with the pile, each with a 1-m thickness, the following parameters were used:

- Pile-soil friction angle, $\delta = 25$ deg.
- $K_l = 0.7$
- Friction angle at pile tip $= \delta = 25$ deg.

A low value was used to account for the considerable disturbance of the soil along the shaft and specially under the pile tip. A parametric analysis was performed (next section) to assess the sensitivity of the results to this parameter.

Fig. 14 displays the time history of the vibratory force applied in the numerical pile driving simulations. Only the last parcel of the load, between 6.5 and 7.0 s, corresponds to the load applied by the operator at 21 Hz. Only 10 cycles of vibrations were considered in the simulations. The remaining load parcels (before 6.5 s) were considered in this study to obtain a numerical overview of pile driving if lower frequencies were used. The loads for these frequencies (7 frequencies varying from 8 to 21 Hz) are proportional to the square of the frequency which correspond to the mechanism of load generation by a rotating mass.

Fig. 15a displays the time histories of the simulated displacements at the pile head and pile tip for the 7 frequency load parcels. A close-up of the results in the last 10 cycles (21 Hz) in Fig. 15b yield a displacement of about 2.75 mm per load cycle. Fig. 15b also plots the corresponding displacements at the pile tip. For pile driving in 1.5 min at 21 Hz (as in the tests), one gets a total pile penetration of $90 \times 21 \times 0.00275 = 5.2$ m which is overall in good agreement with the measured pile penetration of about 7 m in the same period. The most uncertain parameter is the yield strength of the pile-soil springs. A justifiable minor reduction of the shear strength will improve the estimates as shown in the parametric analyses in the next section.

Fig. 16a displays the numerically simulated axial strain in μm/m and

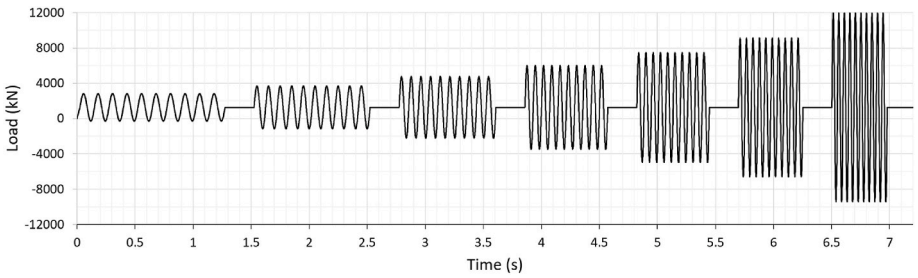

Fig. 14. Forcing function created based on input static and dynamic loads and selected frequencies.

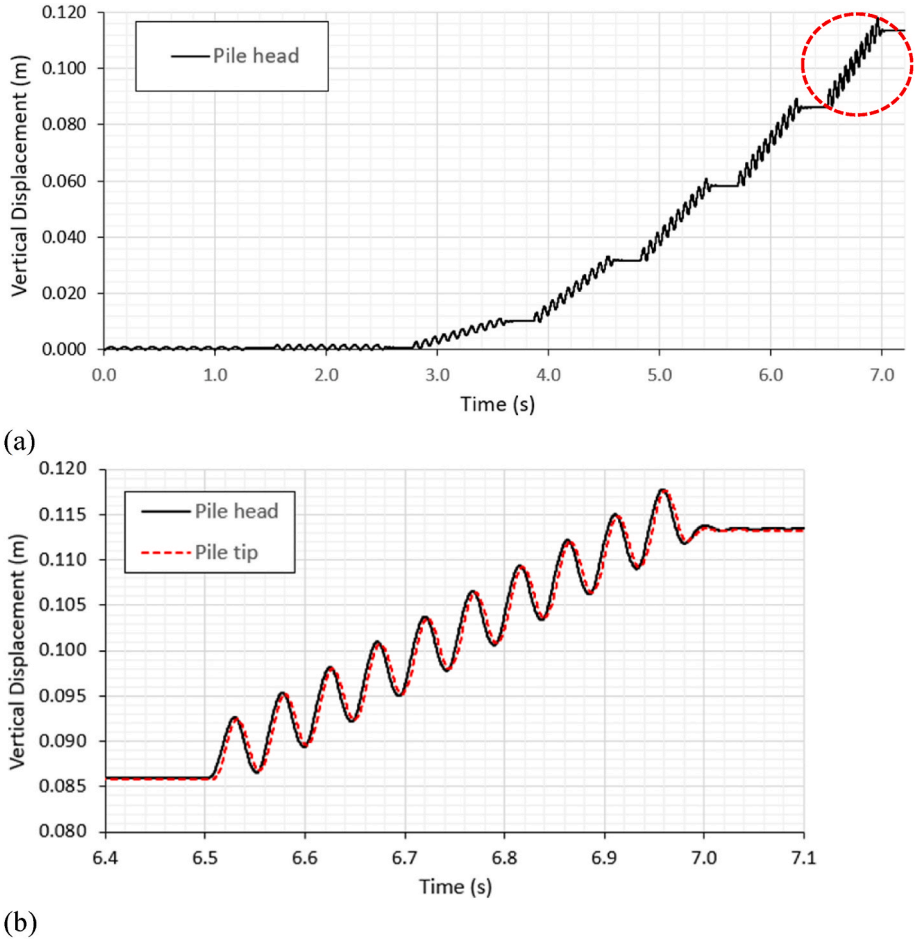

Fig. 15. (a) Simulated displacements at pile head and pile tip, and (b) close-up of displacements for last step of load cycles (21 Hz).

corresponding acceleration in m/s^2 close to the pile head. The data collected from the field tests are also included in Fig. 16b for comparison. There is generally a good agreement between these data despite considerable uncertainties in the parameters. The measured acceleration data display presence of high frequency pulses that could be related to the complex conditions at the pile tip. These pulses, however, do not significantly affect the results which are corroborated by a simple consideration of the applied hammer load and the hammer mass at the pile head.

It should be noted that the small pile penetrations at lower frequencies in Fig. 15 are simply due to the smaller loads at these frequencies related to the mechanism of the vibratory load. If a different driving source that produces the same maximum loads for all frequencies is used, one would get a different picture of driving rates. Such a loading function is shown in Fig. 17 where the maximum load is the same as that used in the experiment (i.e. the last frequency in Fig. 14).

Fig. 18 displays the time history of the simulated displacements at the pile head for the same 7 frequency parcels. The figure clearly illustrates the larger pile driving rate for lower frequencies. This is simply due to the longer time available in each load cycle to drive the pile. The figure demonstrates the importance of time as a parameter in pile driving.

In passing, it is instructive to examine the effect of the natural frequency of the inner soil on pile driving. This is clearly a more important issue in vibratory pile driving compared with impact driving. To this end, the soil profile was replaced by an idealized homogeneous soil with a constant shear wave velocity equal to 150 m/s while keeping the soil strength parameters as in Altenwalde simulations. Using this profile, one can provoke resonance in the soil inside the monopile. With a vibration frequency of about 25 Hz, one could achieve a nondimensional frequency $a_0 = \omega\, d/Vs = 4.5$ which corresponds to the peak impedances in Fig. 7.

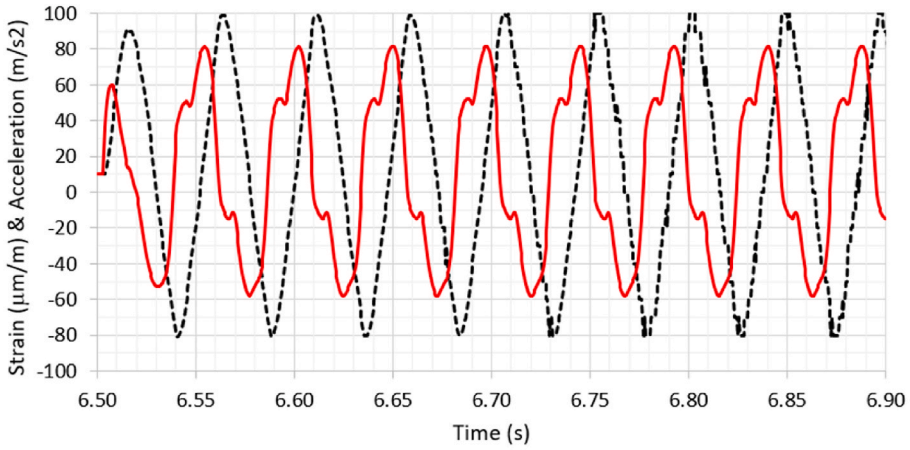

Fig. 16. Simulated (a) and measured (b) time histories of strains (in μm/m) and accelerations (in m/s^2) in a time window corresponding to 21 Hz frequency.

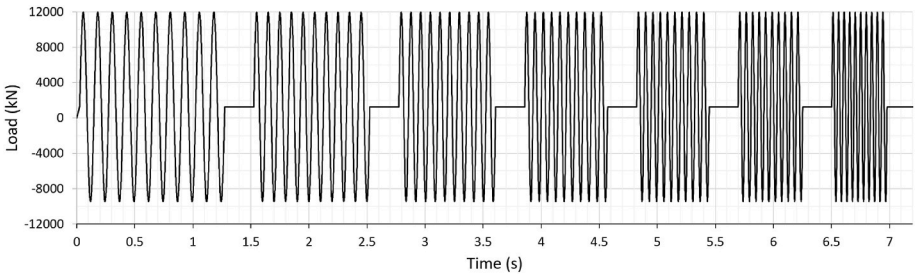

Fig. 17. Artificial forcing function with same maximum force at all vibration frequencies.

Fig. 19 displays the driving rate for frequencies around the natural frequency of the inner soil. It is evident that the combination of large stiffness and damping at the resonant frequency results in a remarkable reduction of pile penetration rate. The figure indicates that at larger frequencies the driving rate goes back to the normal values even though the soil stiffness stays high. The effect of the large stiffness appears to be compensated by the low damping.

4.1. Sensitivity of simulation results to soil parameters

A limited parametric study was performed to highlight the sensitivity of the simulated results to the soil parameters. A friction angle of 25 deg. was used in the preceding simulations which resulted in generally reasonable agreement with the measured data in terms of the rate of driving (pile penetration), axial strain in pile, and peak accelerations.

The most uncertain parameter, at least in the case presented here, is the soil shear strength at the shaft interface which is computed from the shaft-soil friction angle. In the sensitivity analyses, the shaft friction angle was varied from 30° (high estimate) to a value as low as 5 deg. The latter represents a case approaching liquefaction in loose sand. It should be noted that in medium and dense sand, the soil behaviour at large strains could be dilatant which increases the shear strength. This

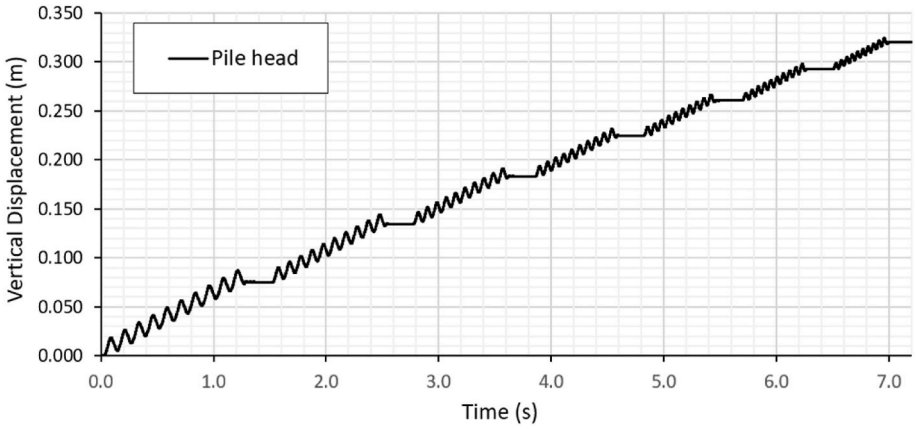

Fig. 18. Simulated pile head displacements for load cycles with same amplitude at different vibratory frequencies.

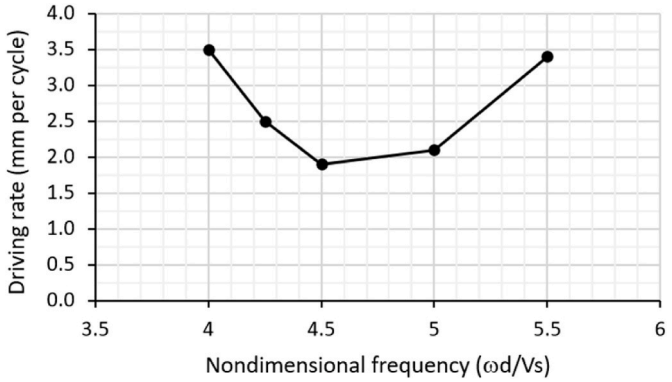

Fig. 19. Pile driving rate at frequencies around natural frequency of soil inside monopile.

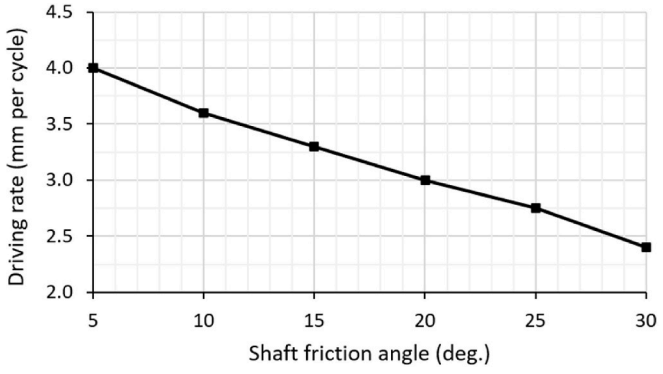

a) Sensitivity to friction angle

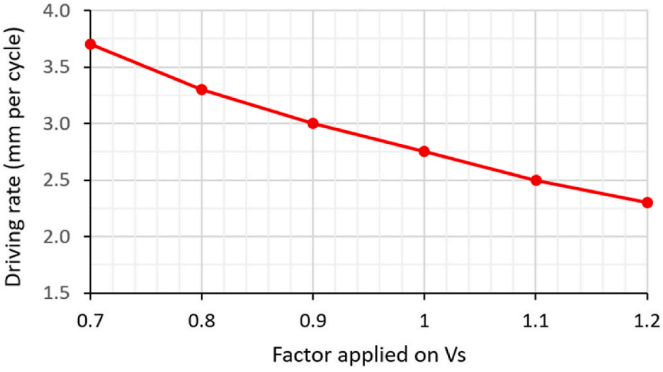

b) Sensitivity to shear wave velocity

Fig. 20. Sensitivity of rate of pile driving to a) shaft friction angle, b) shear wave velocity.

condition cannot be simulated by the simple failure model considered in this study. Special constitutive models, such as the one presented in Ref. [23], could be used in a general finite element framework. A separate sensitivity analysis was carried out for the effect of soil stiffness, represented in terms of change in the shear wave velocity, *Vs*.

Fig. 20a presents the computed rate of driving as function of the shaft friction angle in the range 5–30°. As expected, the driving rate increases as the friction angle is reduced; however, the reduction is not as dramatic as one might intuitively expect. This is partly because of the increased hysteretic damping due to yielding at the pile-soil interface. This is a practically useful observation which indicates that one could use the estimated static bearing capacity as a guideline for determining the capacity of the vibro-hammer.

Fig. 20b displays the sensitivity of the pile driving to the soil stiffness. For this purpose, the shear wave velocity of the soil medium was increased or reduced by a constant factor ranging from 0.8 to 1.1. Note this factor corresponds to about 40% reduction to about 20% increase in the shear modulus, which is practically a large range considering the accuracy in the estimation of the soil modulus in most sites. The figure reveals an increase of about 30% in driving rate in the range considered. While the actual variation in each case depends on several pile-soil parameters, this result again provides a useful practical observation that the soil modulus does not generally have a significant influence on the estimated penetration rate if it is established with reasonable accuracy.

Finally, Fig. 21 displays variation of the driving rate with pile penetration depth. As expected, the driving rate reduces as the pile penetrates more in the soil until it approaches zero. The results of such an analysis can be used in practical design for assessment of pile driveability.

5. Summary and conclusions

This paper presents the numerical code *VibPile* for simulation of the nonlinear dynamic response of large monopiles under harmonic loading and installation by vibration or impact driving. The developed model is verified against the vibro-pile test data collected at Altenwalde, Germany. The analyses indicate a considerable increase of pile stiffness and damping at frequencies close to the natural frequency of the soil inside the pile. While the stiffness remains relatively high for higher

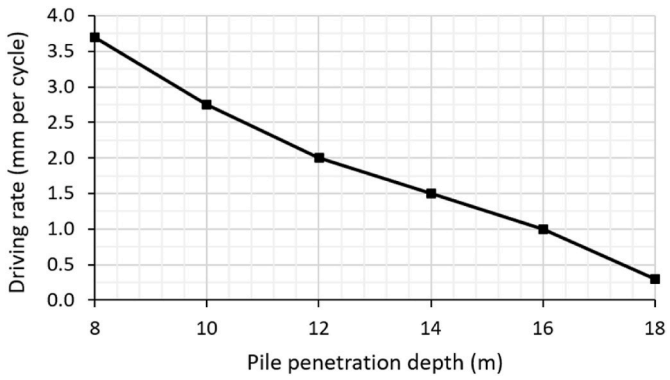

Fig. 21. Pile driveability analysis: driving rate as function of depth.

frequencies, the radiation damping is reduced. The simulation of vibro-installation indicates remarkable reduction in the pile driving rate close to the natural frequency of the inner soil.

The sensitivity analyses indicate that the pile driving rate increases as both the shear wave velocity of the soil and the cyclic shear strength at the pile-soil interface (alternatively, the friction angle at the pile-soil interface in sandy soil) reduce. However, between these parameters, the former represents less uncertainties in the simulations in a well-characterised site where one would expect only minor variations in the shear wave velocity profile. On the other hand, there is generally more uncertainty in the undrained cyclic shear strength in both clayey and sandy soils. The pore pressures generated during driving could remarkably change the shear strength at the pile soil interface, especially in loose sand with possibility of local liquefaction. A careful assessment of the shear strength under large cyclic strains is the key to a reliable estimation and optimization of vibro-pile driving.

Author statement

Amir M. Kaynia: Conceptualization, Methodology, Software, Writing- Original draft preparation. Jan Hebig: Experiment, Data collection, Validation. Taisiya Pein: Site investigation, Experiment, Review and Editing. Yunsup Shin: Model parameters, Review and Editing.

Declaration of competing interest

The authors declare that they have no known competing financial interests or personal relationships that could have appeared to influence the work reported in this paper.

Acknowledgement

This paper is based on a research work partially financed by the grant Nr 0324231B from the German ministry of economic affairs awarded to IWES. The model *VibPile* presented here was developed by the first author when he was at NGI through a research project with IWES.

References

[1] Smith EAL. Pile driving analysis by the wave equation. J Soil Mech Found Div ASCE 1960;86(SM1):35–61.
[2] Goble GG, Rausche F. Pile driveability predictions by CAPWAP, 1st int. Conf. Numerical methods in offshore piling. London: ICE; 1980. p. 29–36.
[3] Randolph MF. Impact – manual, Dynamic analysis of pile driving. 2008.
[4] De Josselin De Jong G. Wat gebeurt er in de grond tijdens het heien (What happens in the soil during pile driving). Ingenieur 1956;68:B77–88 [Breda, The Netherlands].
[5] Rausche F, Goble GG, Likins G. Dynamic determination of pile capacity. J Geotech Eng ASCE 1985;111:367–83.
[6] Baranov A. On the calculation of excited vibrations of an embedded foundation. Vopr Dyn Prochnocti 1967;No. 14:195–209. Polytech. Inst. of Riga.
[7] Novak M. Dynamic stiffness and damping of piles. Can Geotech J 1974;11(4):574–98.
[8] Gazetas G, Dobry R. Simple radiation damping model for piles and footings. J Eng Mech.Div, ASCE 1984;110:937–56.
[9] Mylonakis G. Winkler model for axially loaded piles. Geotechnique 2001;51(5):455–61.
[10] Crispin JJ, Mylonakis GE. In: Kaynia AM, editor. Simplified models for axial static and dynamic analysis of pile foundations in analysis of pile foundations subject to static and dynamic loading. London: CRC Press; 2021.
[11] Michaelides O, Gazetas G, Bouckovalas G, Chrysikou E. Approximate non-linear dynamic axial response of piles. Geotechnique 1997;48(1):33–53.
[12] Deeks AJ, Randolph MF. Analytical modelling of hammer impact for pile driving. Int J Numer Anal Methods GeoMech 1993;17(5):279–302.
[13] Deeks AJ, Randolph MF. A simple model for inelastic footing response to transient loading. Int J Numer Anal Methods GeoMech 1995;19(5):307–29.
[14] Holeyman A, Bertin R, Whenham V. Impdedance of pile shafts under axial vibratory loads. Soil Dynam Earthq Eng 2013;44:115–26. https://doi.org/10.1016/j.soildyn.
[15] Dierssen G. Ein Bodenmechanisches Modell zur Beschreibung der Vibrationsrammung in Körnigen Böden. Karlsruhe, Germany: Doctoral thesis, University of Karlsruhe; 1994 (in German).
[16] Massarsch RK, Wersäll C, Fellenius BH. Vibratory driving of piles and sheet piles – state of practice. Proc Inst Civil Eng – Geotech Eng 2021. https://doi.org/10.1680/jgeen.20.00127.
[17] Gattermann J, Herwig V, Moormann C. VIBRO Projekt Vergleich des lateralen Tragverhaltens von vibrierten und geschlagenen Stahlrohrpfählen in sandigen Böden. Pfahl-Symposium 2015, Mitteilungen des Instituts für Grundbau und Bodenmechanik. Heft: Technische Universität Braunschweig; 2015. p. 99 (in German).
[18] Pein T, Monaco P, Amoroso S, Marchetti D. Comparisons of shear wave velocity measurements using sdmt and other in situ techniques at well-documented test sites. In: Proc. 7th int. Conf. On earthquake geotechnical engineering (ICEGE 2019), june 17-20 2019, rome, Italy. CRC Press; 2019. p. 4420–8. 2019.
[19] Kaynia AM, Kausel E. Dynamics of piles and pile groups in layered soil media. Soil Dynam Earthq Eng 1991;10(8):386–401.
[20] Park J, Kaynia AM. Stiffness matrices for fluid and anisotropic soil layers with applications in soil dynamics. Soil Dynam Earthq Eng 2018;115:169–82. https://doi.org/10.1016/j.soildyn.2018.06.030. 2018.
[21] Petroleum Institute American. Recommended practice for planning, designing and constructing fixed offshore platforms - working stress design. API RP 2A-WSD; 2000.
[22] Chopra A. Dynamics of Structures. *Theory and applications to earthquake engineering.* New Jersey, USA: Prentice Hall; 2001. 0130869732.
[23] Liu HY, Kaynia AM. Characteristics of cyclic undrained model SANISAND-MSu and their effects on response of monopiles for offshore wind structures. Geotechnique 2021:1–16. https://doi.org/10.1680/jgeot.21.00068.